Applied Physics A (2022) 128:700
https://doi.org/10.1007/s00339-022-05842-0

Applied Physics A
Materials Science & Processing

Investigation photoelectric characteristics of ZnO/*p*-Si heterojunction structure modification with PCBM

Murat Yıldırım[1] · **Adem Kocyigit**[2]

Received: 24 March 2022 / Accepted: 2 July 2022 / Published online: 20 July 2022

Abstract

[6,6]-Phenyl C61-butyric acid methyl ester (PCBM) is a good electron transport material and can be employed in optoelectronic application. To understand the effect of the amount ratio on the capacitive behaviors, the pristine ZnO, 3%, 5% and 10% amounts PCBM (low amount) added ZnO interfacial layered Al/ZnO:PCBM/*p*-Si heterojunction structures have been fabricated by sol–gel spin-coating method and characterized by X-ray diffraction (XRD), capacitance–voltage (*C-V*) and conductance-voltage (*G-V*) measurements for the frequency range between 10 kHz and 1 MHz. Some electrical parameters of the pristine ZnO and various PCBM added ZnO interlayered devices have been calculated from $1/C^2$-*V* (1/capacitance^2-voltage) plots for various frequencies. Moreover, capacitance transient (*C-t*) and conductance-transient *(G-t*) measurements of the Al/ZnO:PCBM/*p*-Si devices have been performed for various light illumination intensities from 20 to 100 mW/cm^2 with 20 mW/cm^2 increments under light illumination which has whole spectral matching. The results revealed that PCBM amount has a great effect on capacitance and conductivity values of the Al/ZnO:PCBM/*p*-Si devices.

Keywords Heterojunction structures · *C-V* characterization · Al/ZnO:PCBM/*p*-Si devices · Photosensing

1 Introduction

Metal-oxide semiconductors have been playing a big role in the development of optoelectronic devices such as photovoltaic cells, photodetectors and photodiodes owing to their high electron mobility, high chemical stability and good optical properties [1, 2]. In photodiodes, metal-oxide semiconductors are usually deposited on silicon (Si) substrates to obtain a junction. Many oxide semiconductors such as TiO_2, NiO, CdO, SnO_2 and ZnO have been used in photodiode architectures. Balakarthikeyan et al. reported photodetector performance of pure NiO and NiO:Cu-based photodetectors with different concentrations of Cu dopants [3]. CdO/*p*-Si photodiodes were produced and characterized by Al Orainy and Hendi [1]. TiO_2/SiO_2/*p*-Si heterojunction diodes were studied for photoconductivity behavior by Zhou et al.[4]. SnO_2-based photodetection was studied by Das Mahapatra et al. [5]. Yakuphanoglu et al. [6] reported an analysis of electrical and photovoltaic properties of the ZnO/*p*-Si photodiodes.

Among the metal-oxide semiconductors, ZnO has taken a great interest because of its excellent properties such as wide bandgap (3.37 eV), high chemical stability, low cost, environmentally friendly and non-toxicity [7, 8]. Furthermore, ZnO has widely been used in gas sensors, solar cells, photocatalysts and photodiodes. ZnO thin films have been fabricated with many different methods in the literature. Magnetron sputtering method was employed to produce ZnO thin films by Gao and Li [9]. ZnO thin films were grown via molecular beam epitaxy method by Chen et al. [10]. The pulsed laser deposition method was employed to obtain ZnO thin films by Zeng et al. [11]. Chemical-vapor deposition technique was applied in order to deposit ZnO thin films on fused quartz by Tan et al. [12]. Chemical spray pyrolysis is another method to obtain ZnO thin film employed by Ayouchi et al. [13]. Among these methods, sol–gel spin coating is the cheapest and easiest method for obtaining ZnO thin films [14].

Building a *p–n* junction based on *n*-type ZnO film deposited on *p*-Si is more useful than indium tin oxide

✉ Adem Kocyigit
adem.kocyigit@bilecik.edu.tr

[1] Department of Biotechnology, Faculty of Science, Selcuk University, 42130 Konya, Turkey

[2] Department of Electronics and Automation, Vocational High School, Bilecik Şeyh Edebali University, 11000 Bilecik, Turkey

(ITO) layers due to high cost factors [15]. Thus, employing ZnO in a junction-based device can decrease cost of device. The working mechanism of the metal-oxide based *p–n* junction is that photons transmitted through one conductivity type of metal oxide are gathered in the depletion region of another conductivity type of semiconductor. To improve the electrical properties of photodiodes, doping with inorganic and organic materials is usually a chosen technique. Karataş et al. [16] investigated electrical properties of ruthenium-doped ZnO/*p*-Si heterostructure diodes. Baturay et al. [17] studied gadolinium-doped ZnO/*p*-Si diodes with *I-V* and *C-V* characteristics. Yıldırım et al. [18] investigated indium-doped ZnO/*p*-Si photodiodes via electrical characterizations. The current transient measurements highlighted that indium doping provided to increase of light response. The *C–V* measurements have imparted that the capacitance values are a dominant function of the frequency and voltage for various indium doping levels.

Doping of the metal-oxide semiconductors with organic materials have attracted considerable attention, recently. Organic materials such as [6,6]-Phenyl C61-butyric acid methyl ester (PCBM) is used commonly in organic photovoltaic cells. Polymer and PCBM heterojunction solar cells exhibit long term stability and present low-cost power production [19]. PCBM is the soluble derivative of buckminsterfullerene (C60) which was developed and mainly used as an electron acceptors in optoelectronic devices by Hummelen et al. [20]. Yakuphanoğlu fabricated a *p*-Si/PCBM photodiodes and investigated their electronic and photovoltaic properties via *I-V* and *C-V* characterizations [21]. Gullu et al. and Öztürk investigated the electrical properties of PCBM:ZnO interlayered Al/PCBM:ZnO/*p*-Si photodiodes [22, 23]. Demirezen et al. investigated dielectric behaviors of the Al/PCBM/NiO:ZnO/*p*-Si structures depending on the frequency changes [24].

The study focuses on the capacitive behaviors of the Al/ZnO/*p*-Si devices for the 0%, 3%, 5% and 10% PCBM amounts. According to our best knowledge, there is no any study to work on *C-V* characteristics of the Al/ZnO:PCBM/*p*-Si devices depending on various PCBM amount in the heterostructure for various frequency and light illumination conditions [25–33]. The aim of choosing low amounts PCBM amount is to protect the diode behavior at reverse biases and to provide high amount of capacitance. The Al/ZnO:PCBM/*p*-Si devices were characterized via *C-V* measurements in a wide range frequency and voltage. The electrical and photo-response measurements of fabricated photodiodes were performed, and their photocapacitance and photoconductance behaviors were also studied by using a FYTRONIX 7000 solar simulator which adjusted the light intensity automatically from 20 to 100 mW/cm^2 under light [34].

2 Materials and methods

The heterojunction structures were prepared as follows: PCBM, which was purchased commercially, was dispersed in 1–2 dichlorobenzene (25 g/L concentration) and mixed for 3 h at 60 °C in a dried nitrogen atmosphere. Then, $Zn(C_2H3O_2)2{\cdot}2H_2O$ was dissolved in methanol as 0.2 M and added 3%, 5%, and 10% molar ratios of PCBM into the ZnO solution. After the interaction of PCBM with ZnO, a ruby red color was observed that moves away from red-brown. After this step, 2 cm^2 *p*-Si substrate pieces (5–10 Ω cm resistivity, 600 mm thickness and (111) plane orientation) were cut, and they were ultrasonically cleaned in an ultrasonic bath by acetone, isopropanol and distilled water. Then, HF:H_2O (1:10) solution was applied to the surface of the pieces for 30 s. After cleaning, a 100 nm aluminum coating was deposited on the back side of the wafer pieces by thermal evaporation method for ohmic contacts. The pieces were annealed in N_2 medium for 5 min at 570 °C to achieve ohmic contact between Al and *p*-Si after ohmic contact process [35]. The various amounts of PCBM with ZnO suspensions were coated on the front side of the wafer pieces by spin-coating method at 3000 rpm spin speeds and 30 s. Each of deposited pieces were annealed on a hot plate at 150 °C to dry solvent and heal crystal behaviors. This low-temperature treatment can provide to obtain crystalline ZnO structure and protect PCBM [36–38]. Then, Al was evaporated on the PCBM added ZnO layers via a hole array mask as 7.85×10^{-3} cm^2 circle areas by thermal evaporation method for the metallic contacts. In these devices, ZnO reveals only a low *n*-type conductivity. PCBM serves the ZnO to obtain electrons from the metal and to transfer them to the *p*-Si. Thus, the pristine ZnO interlayered and 3%, 5% and 10% amounts PCBM (low amount) added ZnO interfacial layered Al/ZnO:PCBM/*p*-Si devices were fabricated, and they were called as Al/ZnO/*p*-Si, Al/ZnO:3%PCBM/*p*-Si, Al/ZnO:5%PCBM/*p*-Si and Al/ZnO:10%PCBM/*p*-Si, respectively. The thicknesses of the ZnO, ZnO:3%PCBM, ZnO:5%PCBM, ZnO:10%PCBM layers were determined as 212 nm, 227 nm, 232 nm and 238 nm, respectively by Dektak profilometer. The schematic illustration of the fabricated devices as well as light illumination diagram is shown in Fig. 1. The surface morphology of the ZnO:PCBM interlayer have been studied by scanning electron and atomic force microscopies in our previous work and confirmed as a good interlayer for metal–semiconductor heterojunctions [22].

The X-ray diffraction (XRD) patterns of ZnO:PCBM interlayer has been recorded by a Bruker Advance D8 XRD (Cu α source with 1.5406 Å wavelength). The *C-V* and *G-V* analyses were performed by a computer-controlled Keithley 4200 semiconductor characterization

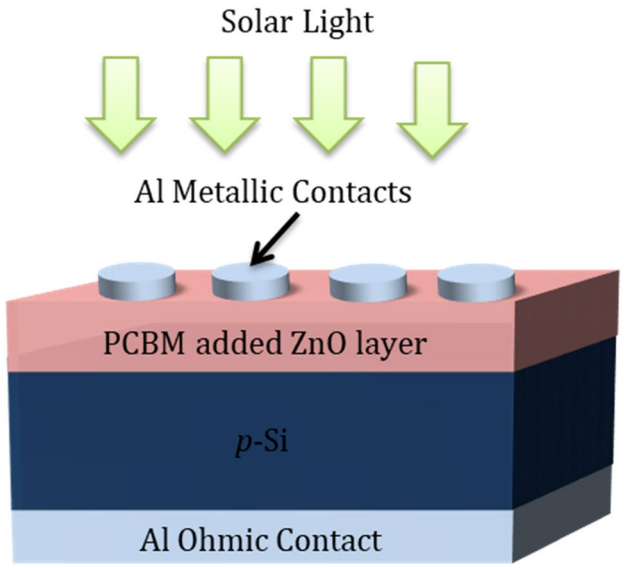

Fig. 1 Schematic illustration of the Al/ZnO:PCBM/*p*-Si devices under light illumination

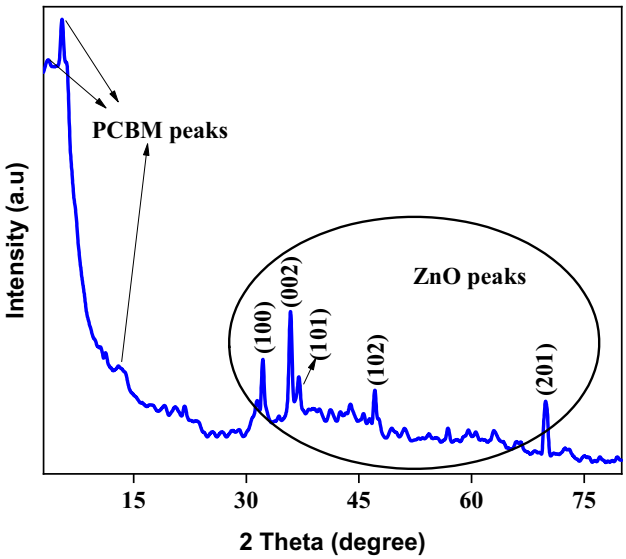

Fig. 2 XRD pattern of ZnO:PCBM interlayer

system under dark for wide range frequency (10 kHz to 1 MHz) and voltage (±5 V). The transient measurements were achieved by 5 s dark and 5 s light exposure for various light illumination intensities. The wavelength of the light is in between the 300 nm and 1200 nm.

3 Results and discussion

XRD patterns of the ZnO:PCBM interlayer are given in Fig. 2. The characteristic ZnO peaks clearly have been seen for various ZnO orientations [39]. Also, PCBM peaks can be detected from XRD patterns for PCBM on *p*-Si substrate [40]. This result highlighted that ZnO:PCBM interlayer exhibited crystalline structure in nature.

The *C-V* graphs of the pristine ZnO and various PCBM added Al/ZnO:PCBM/*p*-Si devices are presented in Fig. 3a–d for the frequency range of 10 kHz and 1 MHz. The devices clearly exhibited accumulation, depletion and inversion region according to *C-V* characteristics. While the changing higher capacitance values with changing frequency exhibit accumulation region, the sudden decreases at the capacitance values show depletion region of the Al/ZnO:PCBM/*p*-Si devices. The region, which is no any change with frequency, shows inversion region. All devices have capacitance peaks in the accumulation region because of series resistance and interface states effects [41, 42]. Furthermore, the capacitance values of the devices did not change in the inversion region with changing frequency. The peak intensities decreased with the increase of the frequency due to the fact that AC signals cannot be followed by the interface states towards higher frequencies [43–45]. The observed peak and shifting their position in the *C-V* plots can be attributed to the existence of surface states at junction, their special distribution in the forbidden bandgap of semiconductor and their restructure and reordering under electric field and series resistance of the device [46]. The Al/ZnO/*p*-Si device has two peaks at lower frequencies, and one broad peak at higher frequencies as shown in Fig. 1a. The Al/ZnO:3%PCBM/*p*-Si device has peaks in the medium accumulation region, but there are increasing negative capacitance values with decreasing frequency in the higher reverse biases. These negative capacitance values seen in the graph can be attributed to the injection of the minority carriers or electron acceptor behaviors of PCBM layers [47]. On the other hand, it is explained that the observation of negative capacitance in the accumulation region is important, because it implies that an increment in bias voltage produces a decrease in the number of charges on the electrodes [48].

The negative capacitance values also have been seen in the Al/ZnO:5%PCBM/*p*-Si and Al/ZnO:10%PCBM/*p*-Si devices for only low frequency values. The reason for the negative capacitance especially at low frequencies can be attributed to PCBM-ZnO interface owing to fact that the ZnO behaves a kind of *n*-type conductivity and provide electrons to the Al metallic contacts [7]. Moreover, a decrease in capacitance values was generally seen with the increasing of PCBM amount due to increasing charge

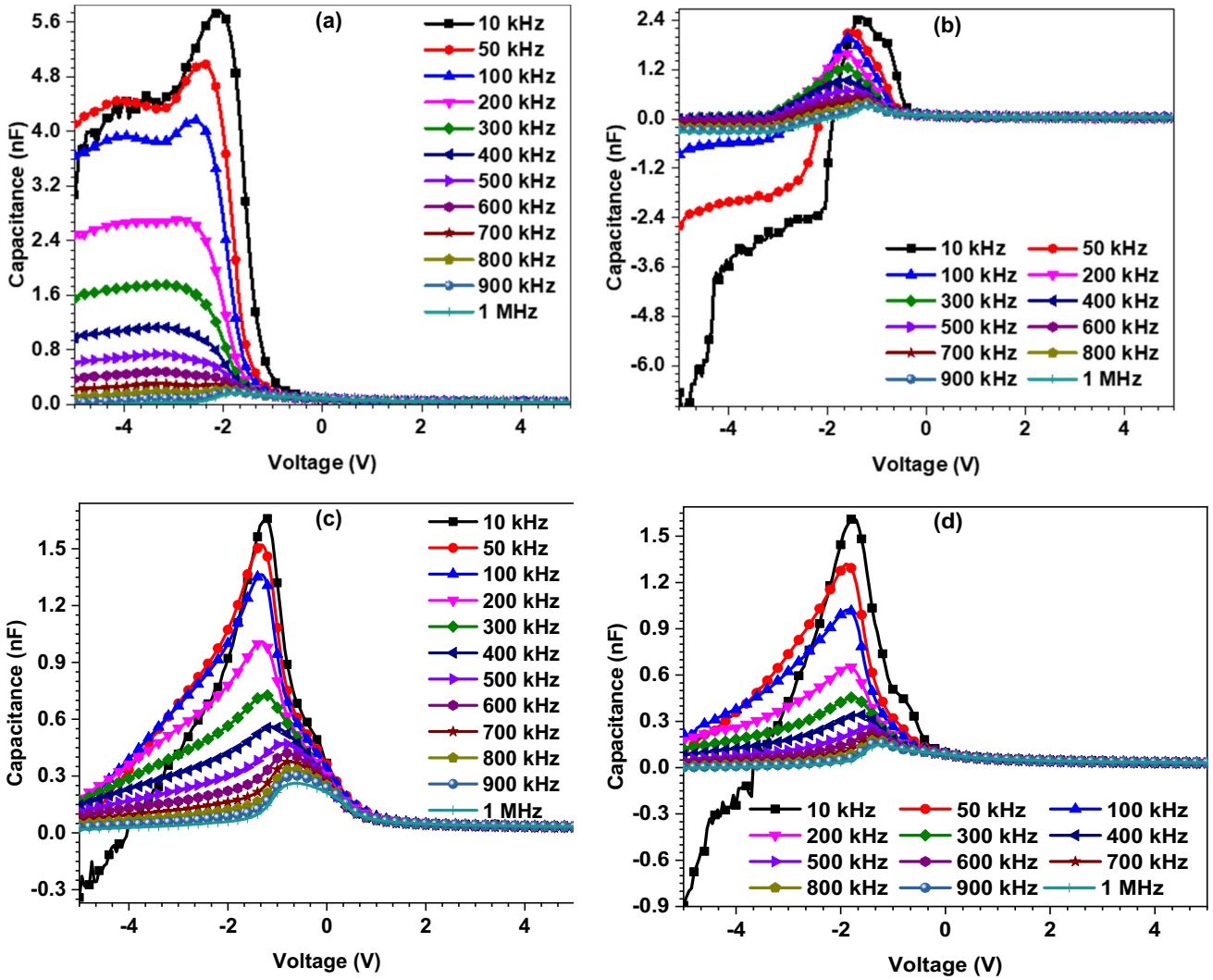

Fig. 3 *C–V* characteristics of the (**a**) Al/ZnO/*p*-Si (**b**) Al/ZnO:3%PCBM/*p*-Si, (**c**) Al/ZnO:5%PCBM/*p*-Si and (**d**) Al/ZnO:10%PCBM/*p*-Si devices

transport [49, 50]. These changes at the various amount PCBM added Al/ZnO:PCBM/*p*-Si devices highlight that the magnitude of capacitance can be controlled with a PCBM material amount.

Figure 4a–d indicates *G-V* graphs of the Al/ZnO/*p*-Si and various PCBM amounts added Al/ZnO:PCBM/*p*-Si devices for the frequency range of 10 kHz and 1 MHz. The conductance values exhibited increasing profile with the increasing frequency for Al/ZnO/*p*-Si and Al/ZnO:5%PCBM/*p*-Si devices and increasing reverse bias. Furthermore, the conductance values increased from 0 to higher negative biases for each frequency of Al/ZnO/*p*-Si device but stayed almost the same for Al/ZnO:5%PCBM/*p*-Si device for higher frequencies after a sudden increase of the conductance. There are some fluctuations at the conductance values for the Al/ZnO:3%PCBM/*p*-Si and Al/ZnO:10%PCBM/*p*-Si devices because the conductance values decreased from 10 to 100 kHz as shown in Fig. 4b, d, and then increased up to 1 MHz frequency. This fluctuation can be depended on the measurement errors or non-uniform film structure of the PCBM added ZnO layers [2]. The conductance values stayed almost constant depending on voltage for the higher reverse bias region in the case of the PCBM-added ZnO interlayered devices. The remaining constant with increasing reverse bias can be attributed to electron transport mechanism of the PCBM [51]. All devices clearly exhibited a sudden decrease towards forward biases. The reason of a sudden decrease for all devices is due to fast depletion of the charge carriers, and this region is called depletion region [52]. Increasing of the conductance values with the increasing of frequency can be attributed to the existence interface states [1]. Moreover, Al/ZnO:3%PCBM/*p*-Si device has higher conductance values than others. After this amount level, the

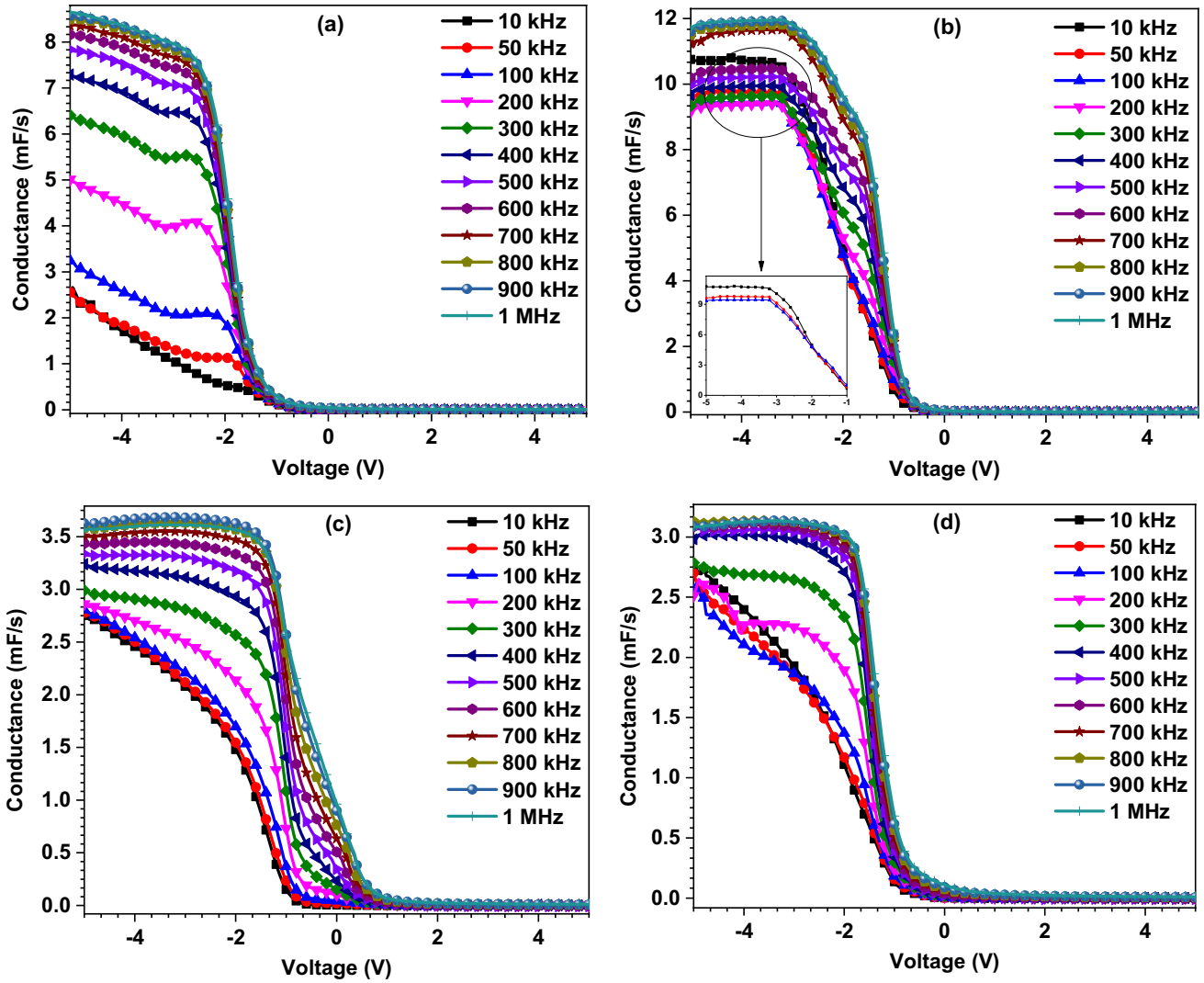

Fig. 4 *G–V* characteristics of the (**a**) Al/ZnO/*p*-Si (**b**) Al/ZnO:3%PCBM/*p*-Si, (**c**) Al/ZnO:5%PCBM/*p*-Si and (**d**) Al/ZnO:10%PCBM/*p*-Si devices

maximum conductance values decreased with increasing the PCBM. The decrease at the conductance values in the accumulation region with increasing PCBM amount level can be attributed to electron transport mechanism of the PCBM.

The $1/C^2$-V plots exhibit straight line and allow the calculation of some parameters such as Fermi level (E_F), barrier height (Φ_b), depletion layer width (W_d), maximum electric field (E_m) and the concentration of the acceptor atoms (N_a) for *p*-Si [53]. The Φ_b values are obtained by the following equation from the $1/C^2$-V plots [54]:

$$\Phi_b(C-V) = (V_d + E_F) - \Delta\Phi, \tag{1}$$

where $\Delta\Phi$ and V_d show image force barrier lowering and diffusion potential ($V_d = V_i + kT/q$), which is determined by the sum of the x-intercept of the $1/C^2$-V plot and kT/q, respectively.

The E_F can be calculated by the next formula [55]:

$$E_F = \frac{KT}{q} Ln\left(\frac{N_v}{N_a}\right), \tag{2}$$

where N_v is given by:

$$N_v = 4.82 \times 10^{15} T^{3/2} \left(\frac{m_h^*}{m_0}\right)^{3/2}, \tag{3}$$

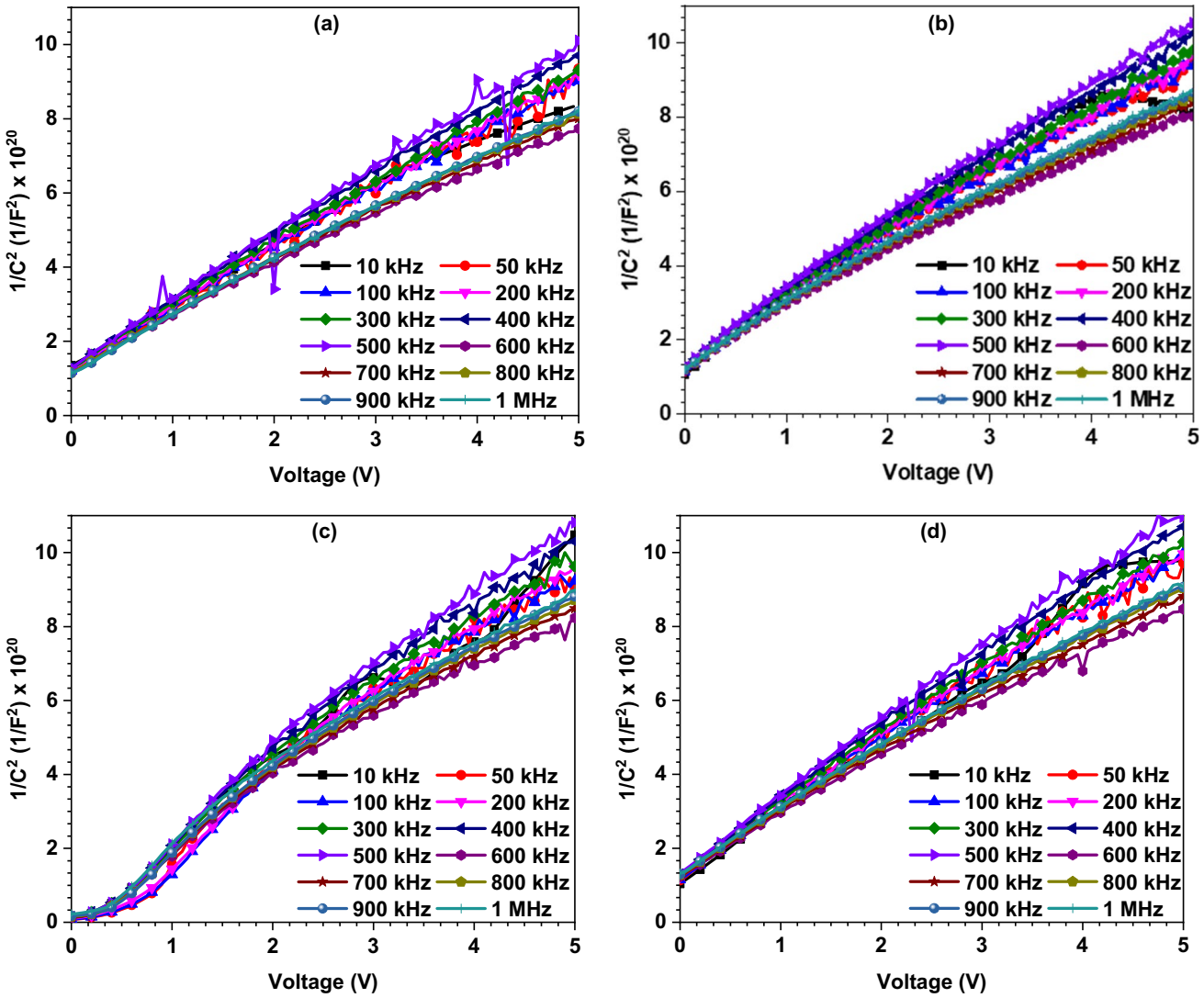

Fig. 5 The $1/C^2$–V plots of the (**a**) Al/ZnO/p-Si (**b**) Al/ZnO:3%PCBM/p-Si, (**c**) Al/ZnO:5%PCBM/p-Si and (**d**) Al/ZnO:10%PCBM/p-Si devices

where m_0 is mass of the electron and m_h^* is effictive mass of hole. The N_a shows acceptor atom concentrations. Other formules of the electrical parameters can be found in the literature [56].

The $1/C^2$-V plots of the Al/ZnO/p-Si and various PCBM amounts added Al/ZnO:PCBM/p-Si devices are exhibited in Fig. 5a–d. All the $1/C^2$-V plots exhibited straight lines for wide range voltages. The deviations from the linearity and not fully linear behavior for the fabricated devices can be ascribed to interfacial layers of the PCBM added ZnO [44]. According to Fig. 5, the slope of $1/C^2$-V curves are in an increasing trend with the increase of frequency for Al/ZnO/p-Si and various PCBM amounts added ZnO interfacial layered Al/ZnO:PCBM/p-Si devices. Some of the electrical parameters of the various PCBM amounts added Al/ZnO:PCBM/p-Si devices are calculated and listed in Tables 1, 2, 3 and 4 for the Al/ZnO/p-Si, Al/ZnO:3%PCBM/p-Si, Al/ZnO:5%PCBM/p-Si and Al/ZnO:10%PCBM/p-Si, respectively. The calculation method of the electrical variables from $1/C^2$-V graphs can be found in the literature [57].

According to Tables 1, 2, 3 and 4, the carrier concentration of acceptor atoms (N_a) for all devices usually decreased towards 500 kHz and then increased suddenly at 600 kHz frequency. After 600 kHz frequency, the N_a values of all devices usually decreased with the increase of frequency. This result can be ascribed to polarization changes or reordering and restructuring of the interface states [58, 59]. The reason of the capacitance in these kinds of devices is attributed to interface states, which are mobile charges, fixed ions, oxide ions, etc. When the frequency increased, they can be reordered and restructured according to changing frequency. When looking at the N_a values totally, almost no so much change is seen with the

Table 1 The electrical parameters of the Al/ZnO/*p*-Si device for various frequencies

f (kHz)	N_a (10^{15} cm^{-3})	R_s (Ω)	Φ_b (eV)	E_F (eV)	E_m ($\times 10^4$ V/cm)	W_d ($\times 10^{-5}$ cm)	N_{ss} (10^9 eV^{-1} cm^{-2})
10	1.180	376.1	0.978	0.187	1.673	9.480	14.4
50	1.203	281.4	1.019	0.186	1.732	9.628	3.49
100	1.218	186.7	1.067	0.186	1.794	9.841	4.23
200	1.233	136.7	1.099	0.186	1.840	9.957	4.06
300	1.188	124.2	1.098	0.186	1.802	10.13	4.97
400	1.152	119.5	1.109	0.187	1.786	10.35	5.12
500	1.132	117.0	1.119	0.188	1.779	10.49	1.70
600	1.425	116.1	1.181	0.182	2.070	9.682	4.48
700	1.404	116.4	1.204	0.182	2.078	9.863	7.90
800	1.384	115.5	1.223	0.183	2.081	10.02	9.65
900	1.384	115.0	1.242	0.183	2.102	10.12	1.11
1000	1.394	114.1	1.252	0.182	2.119	10.13	1.22

Table 2 The electrical parameters of the Al/ZnO:3%PCBM/*p*-Si device for various frequencies

f (kHz)	N_a (10^{15} cm^{-3})	R_s (Ω)	Φ_b (eV)	E_F (eV)	E_m ($\times 10^4$ V/cm)	W_d ($\times 10^{-5}$ cm)	N_{ss} (10^9 eV^{-1} cm^{-2})
10	1.040	92.7	0.9113	0.190	1.497	9.644	31.7
50	1.069	101.8	0.934	0.189	1.543	9.667	12.5
100	1.087	104.2	0.966	0.189	1.590	9.786	10.3
200	1.093	101.3	1.008	0.189	1.638	10.02	9.53
300	1.112	97.5	1.063	0.188	1.708	10.26	9.13
400	1.069	94.6	1.100	0.189	1.709	10.67	9.12
500	1.063	92.9	1.129	0.189	1.731	10.87	5.19
600	1.309	91.5	1.159	0.184	1.959	9.983	7.99
700	1.291	82.8	1.198	0.184	1.984	10.24	10.6
800	1.274	81.9	1.206	0.185	1.978	10.35	11.9
900	1.266	81.4	1.232	0.185	1.997	10.51	12.9
1000	1.266	81.7	1.240	0.185	2.005	10.55	13.9

Table 3 The electrical parameters of the Al/ZnO:5%PCBM/*p*-Si device for various frequencies

f (kHz)	N_a (10^{15} cm^{-3})	R_s (Ω)	Φ_b(eV)	E_F (eV)	E_m ($\times 10^5$ V/cm)	W_d ($\times 10^{-5}$ cm)	N_{ss} (10^{11} eV^{-1} cm^{-2})
10	1.233	363.3	1.171	0.186	1.912	10.34	1.22
50	1.180	349.3	1.015	0.187	1.712	9.695	1.05
100	1.159	324.9	0.924	0.187	1.598	9.235	1.13
200	1.139	293.6	0.919	0.188	1.577	9.280	1.27
300	1.100	276.4	0.890	0.188	1.517	9.252	1.30
400	1.051	259.3	0.879	0.190	1.471	9.381	1.50
500	0.997	248.1	0.850	0.191	1.399	9.419	1.77
600	1.327	237.5	1.016	0.184	1.819	9.166	2.17
700	1.318	231.2	1.131	0.184	1.937	9.807	2.32
800	1.309	226.1	1.181	0.184	1.981	10.09	2.43
900	1.291	222.7	1.186	0.184	1.972	10.18	2.54
1000	1.283	229.1	1.197	0.185	1.976	10.27	2.45

Table 4 The electrical parameters of the Al/ZnO:10%PCBM/*p*-Si device for various frequencies

f (kHz)	N_a (10^{15} cm^{-3})	R_s (Ω)	Φ_b (eV)	E_F (eV)	E_m ($\times 10^5$ V/cm)	W_d ($\times 10^{-5}$ cm)	N_{ss} (10^{10} eV^{-1} cm^{-2})
10	1.188	364.1	1.182	0.186	1.885	10.58	3.03
50	1.093	362.0	1.078	0.189	1.708	10.43	1.48
100	1.087	366.1	1.033	0.189	1.658	10.19	1.37
200	1.069	345.4	1.011	0.189	1.622	10.15	1.32
300	1.046	326.1	1.001	0.190	1.593	10.19	1.42
400	1.002	303.3	0.995	0.191	1.553	10.37	1.52
500	0.967	302.9	0.950	0.192	1.480	10.25	1.29
600	1.266	298.5	1.156	0.185	1.923	10.13	1.64
700	1.233	293.0	1.172	0.186	1.913	10.34	2.08
800	1.203	292.2	1.140	0.186	1.856	10.30	2.33
900	1.188	293.3	1.134	0.186	1.839	10.33	2.58
1000	1.173	295.8	1.110	0.187	1.803	10.26	2.83

increasing of the PCBM amount level because the acceptors are related to directly *p*-Si in the device.

The Φ_b values increased with the increasing of frequency for Al/ZnO/*p*-Si, Al/ZnO:3%PCBM/*p*-Si and Al/ZnO:5%PCBM/*p*-Si devices. However, in the case of Al/ZnO:10%PCBM/*p*-Si, the Φ_b values decreased towards 500 kHz frequency and increased suddenly at 600 kHz frequency, and then again decreased towards 1 MHz frequency. Changes at the Φ_b values with changing frequency can be assigned to the density of interface states and series resistance of the Al/ZnO:PCBM/*p*-Si devices. The E_F values are in increasing tendency with the increasing of frequency up to 500 kHz and decrease suddenly at 600 kHz, and then slightly increase up at 1 MHz frequency. Furthermore, the E_m and W_d values of the fabricated devices exhibited some of changes depending on the frequency. The PCBM amount levels also affected slightly various electrical parameters, but it is hard to claim that the changes are meaningful.

The interface states (N_{ss}) and series resistance (R_s) can be derived from the *C-V* characteristics and can be considered as important for the characterization of metal-semiconductor devices. The correlation of the N_{ss} and frequency can be determined by Hill-Coleman method, which is an approximation method, and thus the N_{ss} is typed by the following formula based on measured capacitance and conductance [60]:

$$N_{ss} = \frac{2}{qA}\frac{(G_m/\omega)_{max}}{((G_m/\omega)_{\max}/C_{0x})^2 + (1 - C_m/C_{0x})^2}, \tag{4}$$

where C_m and G_m are the experimentally measured capacitance and conductance, A is the contact area of the device, q is the charge of the electron, and ω is angular frequency. Also, C_{0x} represents the interface capacitance, and it can be calculated by below formula for strong accumulation region:

$$C_{0x} = C_{ma}\left[1 + \frac{G_{ma}^2}{(\omega C_{ma})^2}\right]. \tag{5}$$

To estimate real value of the series resistance (R_s) for the strong accumulation region, following equation developed by Brews and Nicollian can be employed for metal-oxide semiconductor devices [61]:

$$R_s = \frac{G_{ma}}{G_{ma}^2 + (\omega C_{ma})^2}. \tag{6}$$

The determined N_{ss} and R_s values (in the case of maximum capacitance and conductance) for pristine ZnO and various PCBM added Al/ZnO:PCBM/*p*-Si devices are listed in Tables 1, 2, 3 and 4 for various frequencies. Both the R_s and N_{ss} values usually decreased with the increasing of frequency. While the Al/ZnO:3%PCBM/*p*-Si device has the lowest R_s values, Al/ZnO:5%PCBM/*p*-Si device has the highest ones. According to N_{ss} and R_s values, all the Al/ZnO:PCBM/*p*-Si devices are appropriate for optoelectronic devices. Furthermore, the N_{ss} values are higher at low frequencies due to more effectiveness especially at the low frequencies [62]. The fluctuation at the R_s values with the change of frequency can be ascribed to reordering and restructuring of the N_{ss} values [63].

Figure 6a–d show resistance (R_i)-voltage graphs of the pristine ZnO and various amounts PCBM added Al/ZnO:PCBM/*p*-Si devices for changing frequency. The R_i values were calculated from Eq. (6) for C_m and G_m values for all voltage ranges. The R_i values exhibited peaks in depletion, accumulation and inversion regions for Al/ZnO:5%PCBM/*p*-Si device and depletion regions of other devices because of the existence of the interface states [64]. The peak intensities decreased with the increasing frequency. However, the peak

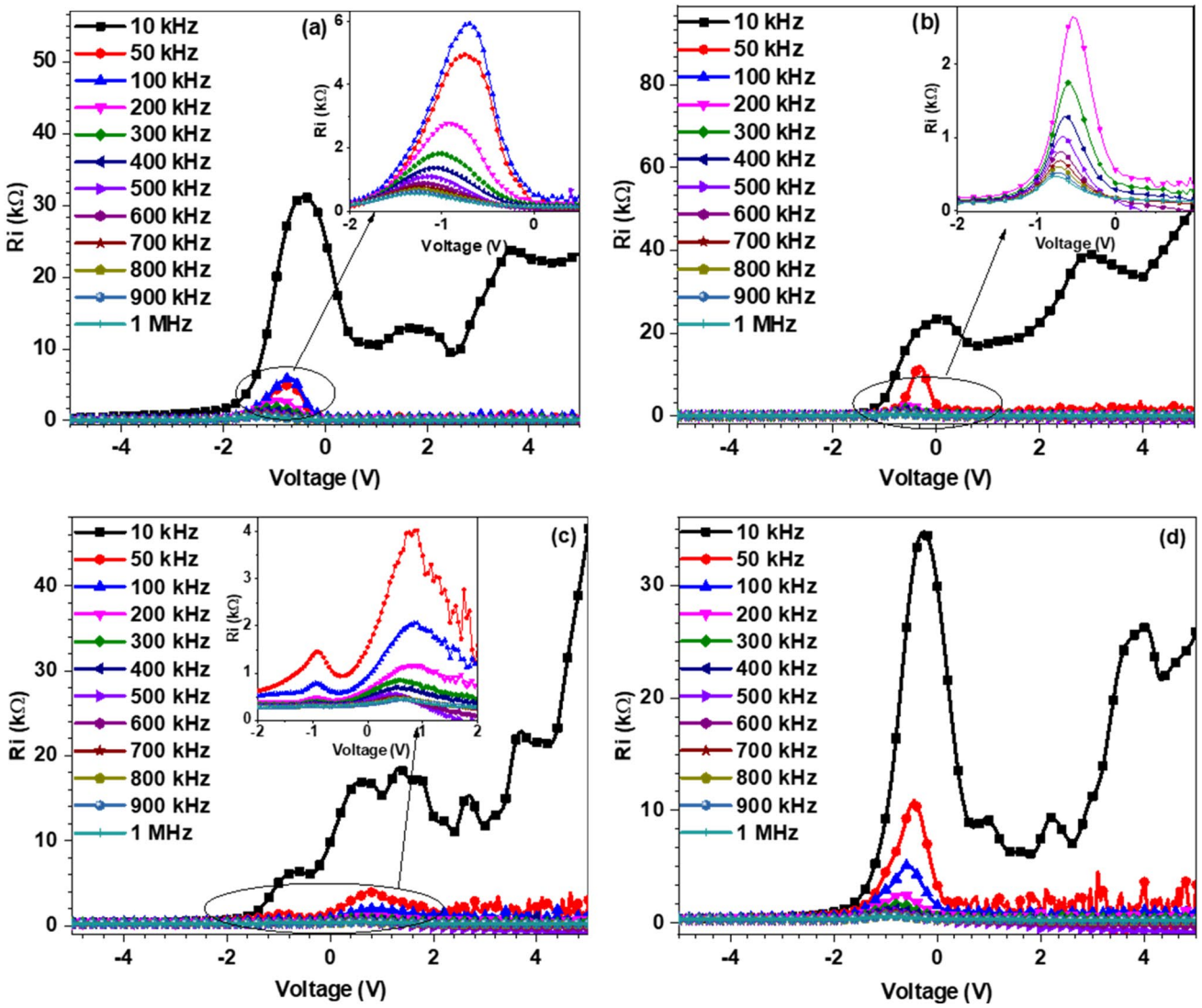

Fig. 6 R_i–V characteristics the (**a**) Al/ZnO/*p*-Si (**b**) Al/ZnO:3%PCBM/*p*-Si, (**c**) Al/ZnO:5%PCBM/*p*-Si and (**d**) Al/ZnO:10%PCBM/*p*-Si devices

positions usually shifted in the direction of the accumulation region. The decrease in peak intensity with the increasing frequency can be ascribed to the fact that the N_{ss} cannot follow the AC signal at higher frequencies [65]. The R_i values did not change in the bigger inversion and accumulation regions for higher frequencies, but there are some changes in the inversion region for lower frequencies. Moreover, the R_i values indicated changes in the range of – 2 to 1 V for all devices except Al/ZnO:5%PCBM/*p*-Si device. The R_i value of this device exhibited two peak regions between – 2 V and 2 V biases due to having more N_{ss} values than the other devices. Furthermore, there is another point should be explained that the R_i values have wide changing area at 10 kHz for all devices. The PCBM amount caused to increase of these wide changes at the R_i values for 50 and 100 kHz frequencies. This result highlighted that the PCBM amount increased the R_i values for lower frequencies in the inversion region due to increasing the N_{ss} values or inhomogeneities in the interface of the devices [66].

Figure 7a–d exhibit the capacitance-transient (*C*-*t*) measurements of the pristine ZnO and various PCBM added Al/ZnO:PCBM/*p*-Si devices for various light illumination intensities per cm^2. *C*-*t* measurements of the Al/ZnO:PCBM/*p*-Si devices were carried out under the increasing light illumination intensity from 20 mW/cm^2 to 100 mW/cm^2 with 20 mW/cm^2 increments. All the devices exhibited capacitance values for increasing illumination due to increasing of the interface states and decreasing the initial values after illumination. However, pristine ZnO device has slow increase at the capacitance values for the lower illumination intensities, which are readily apparent in Fig. 7a. When the light illumination increased from 80 mW/cm^2 to 100 mW/cm^2

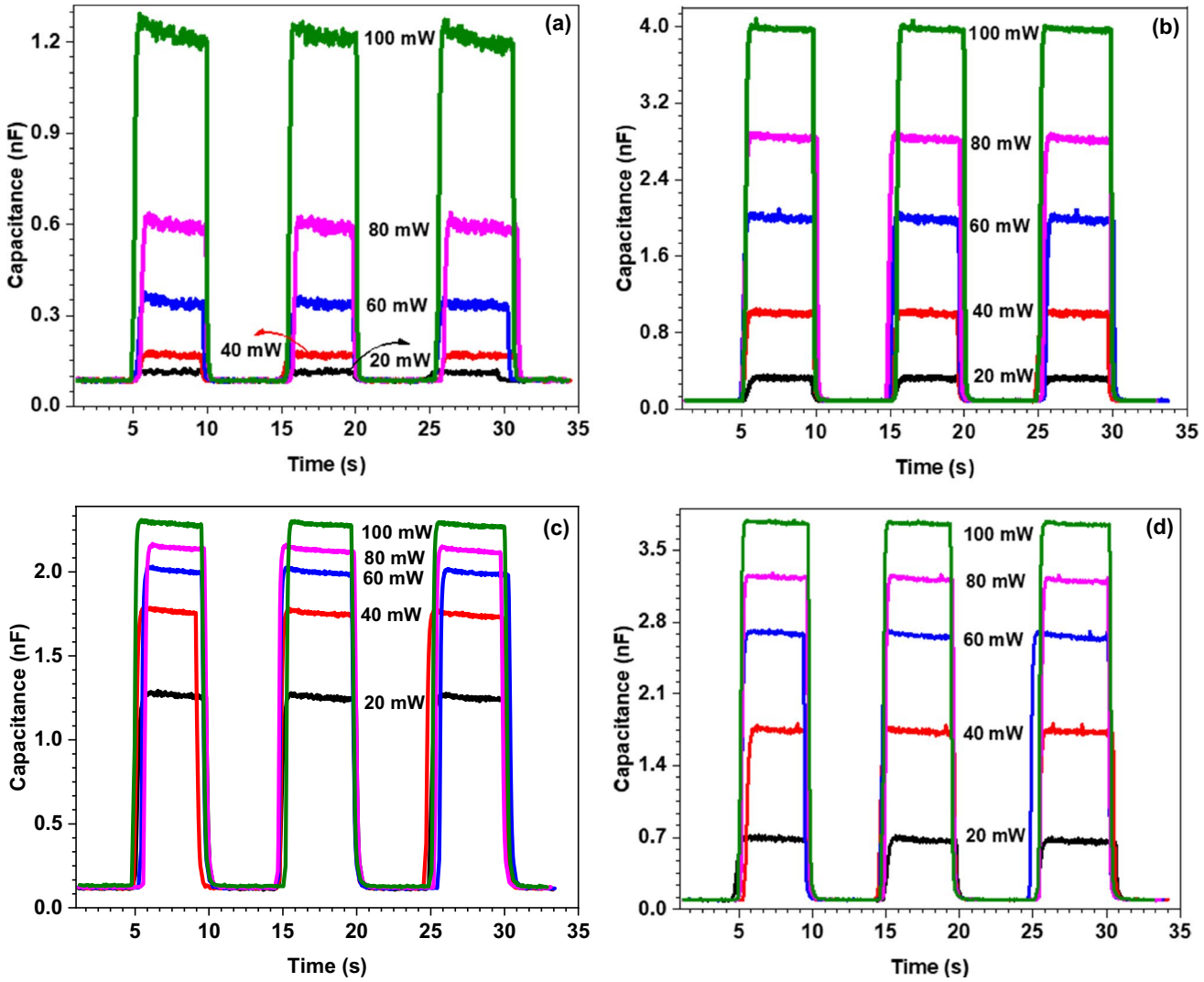

Fig. 7 *C-t* measurement results of the (**a**) Al/ZnO/*p*-Si (**b**) Al/ZnO:3%PCBM/*p*-Si, (c) Al/ZnO:5%PCBM/*p*-Si and (**d**) Al/ZnO:10%PCBM/*p*-Si devices

for the pristine ZnO device, the capacitance value made a sudden and big jump. The Al/ZnO:5%PCBM/*p*-Si device exhibited higher capacitance values at 20 mW/cm^2 power, and then slightly increased for other illumination intensities due to trapped charges. The Al/ZnO:3%PCBM/*p*-Si and Al/ZnO:10%PCBM/*p*-Si PCBM added devices have higher capacitance values as well as almost linear increase with increasing light illumination intensity.

The PCBM amount clearly increased capacitance values due to increasing transport of charge carriers in the interface of the devices and caused temporary capacitance. The reason of the temporarily capacitance is carriers accumulated in the interface of the devices. When the applied voltage increased, the carriers have faster transportation. Thus, the capacitance values decreased. When the light was turned on, the capacity increased rapidly, and when the light was turned off, it suddenly returned to its previous level. The increase of capacitance values with increasing light intensity confirmed that more free charge carriers were produced under illumination and approved photo-capacitive behavior of the devices. The correct amount of the PCBM in the interface is important for the higher photocapacitance behavior. The higher value of the PCBM can be decreased the capacitance values due to fast transportation of the charge carriers. Cho et al. studied the role of additional PCBM insertion between the ZnO ripple layer and active layer of the bulk heterojunction type solar cell [26]. To provide additional PCBM layer caused to increase current homogeneity and decreased trapping of the forming charges due to light illumination on the ZnO interlayer. The light illuminated *C-V* characteristics of the with and without PCBM additional layer devices revealed that additional PCBM layer caused to avoid more

trapping of charge on the ZnO layer and better charge extraction in the interface. Thus, electron–hole recombination was stopped by PCBM layer insertion. Therefore, using of correct amount of PCBM can increase the performance of the heterojunction for various applications. Verma et al., studied *C-V* characteristics of P3HT:PCBM-based BHJ solar cells for contact surface photovoltage as well as associated carrier accumulation at the contact [67]. The *C-V* characteristics of P3HT:PCBM were studied both conventional (transparent anode) and inverted (transparent cathode) constructions under dark and light illumination conditions to obtain built-in voltage and surface photovoltage, respectively. The *C-V* characteristics under illumination revealed peaks behavior with shifting towards lower bias values by increasing illumination intensity.

Figure 8a–d indicate the conductance-transient (*G-t*) measurements of the Al/ZnO:PCBM/*p*-Si devices with and without various amounts of PCBM amount for different light illumination intensities per cm^2. *G-t* measurements were taken under the increasing light illumination intensity from 20 mW/cm^2 to 100 mW/cm^2 with 20 mW/cm^2 increments. The conductance values for all fabricated devices have *G-t* phenomena with exposing light illumination. The pristine ZnO device has a slow, but linear increase with increasing light illumination intensity. However, Al/ZnO:3%PCBM/*p*-Si device has higher conductance values than pristine ZnO device at 20 mW/cm^2 light illumination intensity, and their increase slowed down to higher illumination intensity. In the case of Al/ZnO:5%PCBM/*p*-Si and Al/ZnO:10%PCBM/*p*-Si, the devices have higher conductance values again, and then they have almost linearly increasing profile with the

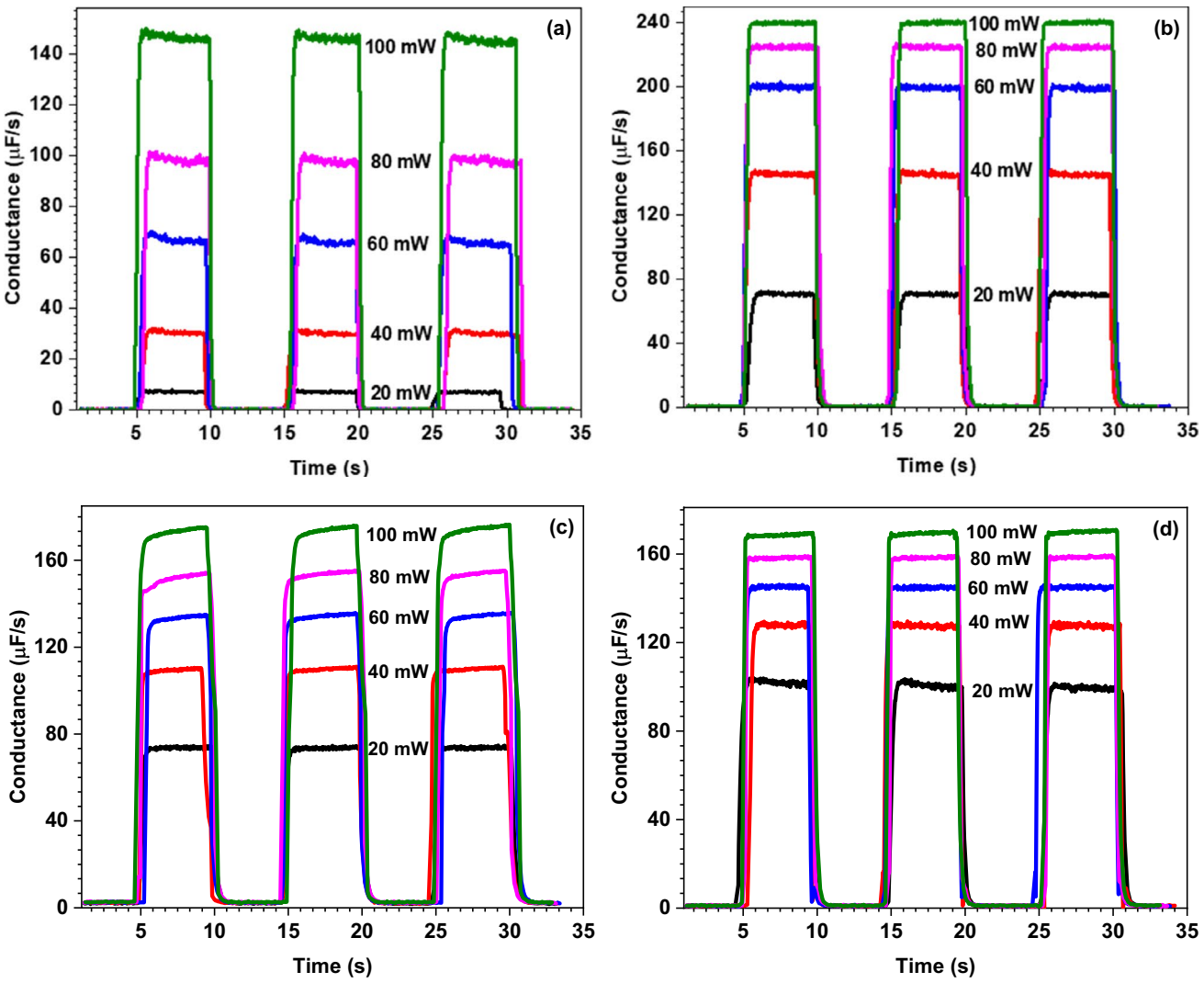

Fig. 8 *G-t* measurement results of the (**a**) Al/ZnO/*p*-Si (**b**) Al/ZnO:3%PCBM/*p*-Si, (**c**) Al/ZnO:5%PCBM/*p*-Si and (**d**) Al/ZnO:10%PCBM/*p*-Si devices

increasing light illumination intensity. The highest conductance values were obtained for Al/ZnO:3%PCBM/*p*-Si device. The PCBM amount level caused to increase the conductance values of the devices due to provide the transportation of the charge carriers easily and without capturing the traps in the interface of the devices.

4 Conclusions

Pristine ZnO and various PCBM amounts added ZnO interlayered Al/ZnO:PCBM/*p*-Si devices were fabricated by sol–gel spin-coating technique. The XRD results of the ZnO:PCBM interlayer confirmed the crystalline structure in nature. The *C-V* and *G-V* measurements were employed to investigate electrical behaviors of the pristine ZnO and various PCBM added Al/ZnO:PCBM/*p*-Si devices for a wide range of frequencies. The capacitance and conductance values of the devices changed depending strongly on the PCBM amount, frequency and voltage changes. The *C-V* characteristics of the Al/ZnO:PCBM/*p*-Si devices revealed peaks behaviors due to the existence of the surface/interface states in the junctions. Negative capacitance behaviors were obtained with adding of PCBM especially for lower frequencies because of injection of minority carriers into junctions. Furthermore, various electrical parameters of the pristine ZnO and various PCBM added devices were obtained from the C^{-2}-V plots, and their electrical properties were discussed in detail according to the frequency and PCBM amount level. *C-t* and *G-t* measurements were performed under different illumination intensities, and these measurements highlight that all the devices can be used as photocapacitor and photoconductor applications.

Author contributions Conceptualization, M.Y.; methodology, M.Y. and A.K.; investigation, M.Y. and A.K.; writing—original draft preparation, M.Y. and A.K.; writing—review, supervision and editing, M.Y. and A.K. All authors have read and agreed to the published version of the manuscript.

Funding This work was supported by Selcuk University BAP office with Project Number 19401034.

Declarations

Conflict of interest The authors declare no conflict of interest.

References

1. R.H. Al Orainy, A.A. Hendi, Fabrication and electrical characterization of CdO/p-Si photosensors. Microelectron. Eng. **127**, 14–20 (2014). https://doi.org/10.1016/j.mee.2014.02.014
2. A. Kocyigit, M. Yılmaz, Ş Aydoğan, Ü. İncekara, The effect of measurements and layer coating homogeneity of AB on the Al/AB/p-Si devices. J. Alloys Compd. **790**, 388–396 (2019). https://doi.org/10.1016/j.jallcom.2019.03.179
3. R. Balakarthikeyan, A. Santhanam, R. Anandhi, S. Vinoth, A.M. Al-Baradi, Z.A. Alrowaili, M.S. Al-Buriahi, K. Deva Arun Kumar, Fabrication of nanostructured NiO and NiO: Cu thin films for high-performance ultraviolet photodetector. Opt. Mater. Amst. **120**, 111387 (2021). https://doi.org/10.1016/j.optmat.2021.111387
4. X. Zhou, L. Wang, X. Zhang, Y. Qiu, Direct and alternating electrical performance of TiO2/SiO2/p-Si heterojunction under visible illumination. Thin Solid Films **718**, 138477 (2021). https://doi.org/10.1016/j.tsf.2020.138477
5. A. Das Mahapatra, D. Basak, Investigation on sub-band gap defects aided UV to NIR broad-band low-intensity photodetection by SnO2 thin film. Sens. Actuators, A Phys. **312**, 112168 (2020). https://doi.org/10.1016/j.sna.2020.112168
6. F. Yakuphanoglu, Y. Caglar, M. Caglar, S. Ilican, ZnO/p-Si heterojunction photodiode by solgel deposition of nanostructure n-ZnO film on p-Si substrate. Mater. Sci. Semicond. Process. **13**, 137–140 (2010). https://doi.org/10.1016/j.mssp.2010.05.005
7. Ü. Özgür, Y.I. Alivov, C. Liu, A. Teke, M.A. Reshchikov, S. Doğan, V. Avrutin, S.J. Cho, H. Morkç, A comprehensive review of ZnO materials and devices. J. Appl. Phys. **98**, 1–103 (2005)
8. Ü. Ozgur, D. Hofstetter, H. Morkoç, ZnO devices and applications: a review of current status and future prospects. Proc. IEEE **98**, 1255–1268 (2010). https://doi.org/10.1109/JPROC.2010.2044550
9. W. Gao, Z. Li, ZnO thin films produced by magnetron sputtering. Ceram. Int. **30**, 1155–1159 (2004). https://doi.org/10.1016/j.ceramint.2003.12.197
10. Y. Chen, D.M. Bagnall, H. Koh, K. Park, K. Hiraga, Z. Zhu, T. Yao, Plasma assisted molecular beam epitaxy of ZnO on c -plane sapphire: Growth and characterization. J. Appl. Phys. **84**, 3912–3918 (1998). https://doi.org/10.1063/1.368595
11. J.N. Zeng, J.K. Low, Z.M. Ren, T. Liew, Y.F. Lu, Effect of deposition conditions on optical and electrical properties of ZnO films prepared by pulsed laser deposition. Appl. Surf. Sci. **197–198**, 362–367 (2002). https://doi.org/10.1016/S0169-4332(02)00425-7
12. S.T. Tan, B.J. Chen, X.W. Sun, W.J. Fan, H.S. Kwok, X.H. Zhang, S.J. Chua, Blueshift of optical band gap in ZnO thin films grown by metal-organic chemical-vapor deposition. J. Appl. Phys. **98**, 013505 (2005). https://doi.org/10.1063/1.1940137
13. R. Ayouchi, F. Martin, D. Leinen, J.R. Ramos-Barrado, Growth of pure ZnO thin films prepared by chemical spray pyrolysis on silicon. J. Cryst. Growth **247**, 497–504 (2003). https://doi.org/10.1016/S0022-0248(02)01917-6
14. S. Ilican, M. Caglar, Preparation and characterization of ZnO thin films deposited. J. Optoelectron. Adv. Mater. **10**, 2578–2583 (2008)
15. J.Y. Lee, Y.S. Choi, J.H. Kim, M.O. Park, S. Im, Optimizing n-ZnO/p-Si heterojunctions for photodiode applications. Thin Solid Films **403–404**, 553–557 (2002). https://doi.org/10.1016/S0040-6090(01)01550-4
16. Ş Karataş, H.M. El-Nasser, A.A. Al-Ghamdi, F. Yakuphanoglu, High photoresponsivity Ru-doped ZnO/p-Si heterojunction diodes by the sol-gel method. SILICON **10**, 651–658 (2018). https://doi.org/10.1007/s12633-016-9508-7
17. S. Baturay, Y.S. Ocak, D. Kaya, The effect of Gd doping on the electrical and photoelectrical properties of Gd:ZnO/p-Si heterojunctions. J. Alloys Compd. **645**, 29–33 (2015). https://doi.org/10.1016/j.jallcom.2015.04.212
18. M. Yıldırım, A. Kocyigit, Characterization of Al/In:ZnO/p-Si photodiodes for various In doped level to ZnO interfacial layers. J.

Alloys Compd. **768**, 1064–1075 (2018). https://doi.org/10.1016/j.jallcom.2018.07.295
19. B. Zimmermann, U. Würfel, M. Niggemann, Longterm stability of efficient inverted P3HT:PCBM solar cells. Sol. Energy Mater. Sol. Cells **93**, 491–496 (2009). https://doi.org/10.1016/j.solmat.2008.12.022
20. J.C. Hummelen, B.W. Knight, F. LePeq, F. Wudl, J. Yao, C.L. Wilkins, Preparation and characterization of fulleroid and methanofullerene derivatives. J. Org. Chem. **60**, 532–538 (1995). https://doi.org/10.1021/jo00108a012
21. F. Yakuphanoglu, Photovoltaic properties of hybrid organic/inorganic semiconductor photodiode. Synth. Met. **157**, 859–862 (2007). https://doi.org/10.1016/j.synthmet.2007.08.012
22. H.H. Gullu, D.E. Yildiz, A. Kocyigit, M. Yıldırım, Electrical properties of Al/PCBM:ZnO/p-Si heterojunction for photodiode application. J. Alloys Compd. **827**, 154279 (2020). https://doi.org/10.1016/j.jallcom.2020.154279
23. T. Öztürk, Effect of various PCBM doping on the interfacial layer of Al/PCBM:ZnO/p-Si photodiodes. J. Mater. Sci. Mater. Electron. **32**, 10180–10193 (2021). https://doi.org/10.1007/s10854-021-05674-3
24. S. Demirezen, H.G. Çetinkaya, Altındal doping rate, interface states and polarization effects on dielectric properties, electric modulus, and AC conductivity in PCBM/NiO:ZnO/p-Si structures in wide frequency range. SILICON **1**, 1–11 (2022). https://doi.org/10.1007/s12633-021-01640-0
25. H. Altan, M. Özer, H. Ezgin, Investigation of electrical parameters of Au/P3HT:PCBM/n-6H–SiC/Ag Schottky barrier diode with different current conduction models. Superlattices Microstruct. **146**, 106658 (2020). https://doi.org/10.1016/j.spmi.2020.106658
26. S. Cho, K.D. Kim, J. Heo, J.Y. Lee, G. Cha, B.Y. Seo, Y.D. Kim, Y.S. Kim, S.Y. Choi, D.C. Lim, Role of additional PCBM layer between ZnO and photoactive layers in inverted bulk-heterojunction solar cells. Sci. Rep. **4**, 1–6 (2014). https://doi.org/10.1038/srep04306
27. S. Demirezen, H.G. Çetinkaya, M. Kara, F. Yakuphanoğlu, Ş Altındal, Synthesis, electrical and photo-sensing characteristics of the Al/(PCBM/NiO: ZnO)/p-Si nanocomposite structures. Sens. Actuators, A Phys. **317**, 112449 (2021). https://doi.org/10.1016/j.sna.2020.112449
28. B. Kadem, R.K. Fakher Alfahed, A.S. Al-Asadi, H.A. Badran, Morphological, structural, optical, and photovoltaic cell of copolymer P3HT: ICBA and P3HT:PCBM. Optik (Stuttg). **204**, 164153 (2020). https://doi.org/10.1016/j.ijleo.2019.164153
29. A.T. Mallajosyula, S. Sundar Kumar Iyer, B. Mazhari, Capacitance-voltage characteristics of P3HT:PCBM bulk heterojunction solar cells with ohmic contacts and the impact of single walled carbon nanotubes on them. Org. Electron. **13**, 1158–1165 (2012). https://doi.org/10.1016/j.orgel.2012.03.018
30. A. Sarkar, A. Bin Rahaman, D. Banerjee, Temperature dependent charge transport studies across thermodynamic glass transition in P3HT:PCBM bulk heterojunction: insight from J-V and impedance spectroscopy. J. Phys. D. Appl. Phys. **51**, 095602 (2018). https://doi.org/10.1088/1361-6463/aaa87c
31. S. Arora, V. Singh, M. Arora, R. Pal Tandon, Evaluating effect of surface state density at the interfaces in degraded bulk heterojunction organic solar cell. Physica B **407**, 3044–3046 (2012)
32. H.H. Gullu, D.E. Yildiz, L. Toppare, A. Cirpan, Electrical characteristics of organic heterojunction with an alternating benzotriazole and fluorene containing copolymer. J. Mater. Sci. Mater. Electron. **31**, 18816–18831 (2020). https://doi.org/10.1007/s10854-020-04421-4
33. Ö. Tüzün Özmen, E. Yağlioğlu, Electrical and interfacial properties of Au/P3HT:PCBM/n-Si Schottky barrier diodes at room temperature. Mater. Sci. Semicond. Process. **26**, 448–454 (2014). https://doi.org/10.1016/j.mssp.2014.04.013
34. F. Aslan, H. Esen, F. Yakuphanoglu, Electrical and fotoconducting characterization of Al/coumarin:ZnO/Al novel organic-inorganic hybrid photodiodes. J. Alloys Compd. **789**, 595–606 (2019). https://doi.org/10.1016/j.jallcom.2019.03.090
35. Z. Çaldıran, Modification of Schottky barrier height using an inorganic compound interface layer for various contact metals in the metal/p-Si device structure. J. Alloys Compd. **865**, 158856 (2021). https://doi.org/10.1016/j.jallcom.2021.158856
36. P.Y. Wu, J. Pike, F. Zhang, S.W. Chan, Low-temperature synthesis of zinc oxide nanoparticles. Int. J. Appl. Ceram. Technol. **3**, 272–278 (2006). https://doi.org/10.1111/j.1744-7402.2006.02091.x
37. S. Bai, J. Hu, D. Li, R. Luo, A. Chen, C.C. Liu, Quantum-sized ZnO nanoparticles: synthesis, characterization and sensing properties for NO2. J. Mater. Chem. **21**, 12288–12294 (2011). https://doi.org/10.1039/c1jm11302j
38. A. Rodrigues, M.C.R. Castro, A.S.F. Farinha, M. Oliveira, J.P.C. Tomé, A.V. Machado, M.M.M. Raposo, L. Hilliou, G. Bernardo, Thermal stability of P3HT and P3HT:PCBM blends in the molten state. Polym. Test. **32**, 1192–1201 (2013). https://doi.org/10.1016/j.polymertesting.2013.07.008
39. M. Bououdina, S. Azzaza, R. Ghomri, M.N. Shaikh, J.H. Dai, Y. Song, W. Song, W. Cai, M. Ghers, Structural and magnetic properties and DFT analysis of ZnO:(Al, Er) nanoparticles. RSC Adv. **7**, 32931–32941 (2017). https://doi.org/10.1039/c7ra01015j
40. C. Wang, H. Hao, D. Hashizume, K. Tajima, Surface-induced enantiomorphic crystallization of achiral fullerene derivatives in thin films. Chem. Sci. **11**, 4702–4708 (2020). https://doi.org/10.1039/d0sc01163k
41. Ö. Sevgili, Y. Azizian-Kalandaragh, Ş Altındal, Frequency and voltage dependence of electrical and dielectric properties in metal-interfacial layer-semiconductor (MIS) type structures. Phys. B Condens. Matter **587**, 412122 (2020). https://doi.org/10.1016/j.physb.2020.412122
42. M. Ulusoy, S. Altındal, Y. Azizian-Kalandaragh, S. Özçelik, Z. Mirzaei-Kalar, The electrical characteristic of an MIS structure with biocompatible minerals doped (Brushite+Monetite: PVC) interface layer. Microelectron. Eng. **258**, 111768 (2022). https://doi.org/10.1016/j.mee.2022.111768
43. M.O. Erdal, M. Yıldırım, A. Kocyigit, A comparison of the electrical characteristics of TiO2/p-Si/Ag, GNR-TiO2/p-Si/Ag and MWCNT-TiO2/p-Si/Ag photodiodes. J. Mater. Sci. Mater. Electron. **30**, 13617–13626 (2019). https://doi.org/10.1007/s10854-019-01731-0
44. M.O. Erdal, A. Kocyigit, M. Yıldırım, The C-V characteristics of TiO2/p-Si/Ag, GNR doped TiO2/p-Si/Ag and MWCNT doped TiO2/p-Si/Ag heterojunction devices. Chinese J. Phys. **64**, 163–173 (2020). https://doi.org/10.1016/j.cjph.2019.12.021
45. Ç.G. Türk, S.O. Tan, Ş Altındal, B. İnem, Frequency and voltage dependence of barrier height, surface states, and series resistance in Al/Al2O3/p-Si structures in wide range frequency and voltage. Phys. B Condens. Matter **582**, 411979 (2020). https://doi.org/10.1016/j.physb.2019.411979
46. S. Kaya, A. Aktag, E. Yilmaz, Effects of gamma-ray irradiation on interface states and series-resistance characteristics of BiFeO3 MOS capacitors. Nucl. Instrum. Methods Phys Res. Sect. B Beam Interact. Mater. Atoms **319**, 44–47 (2014). https://doi.org/10.1016/j.nimb.2013.11.006
47. M. Gökçen, H. Altuntaş, Ş Altındal, S. Özçelik, Frequency and voltage dependence of negative capacitance in Au/SiO2/n-GaAs structures. Mater. Sci. Semicond. Process. **15**, 41–46 (2012). https://doi.org/10.1016/j.mssp.2011.08.001
48. B.K. Jones, J. Santana, M. McPherson, Negative capacitance effects in semiconductor diodes. Solid State Commun. **107**, 47–50 (1998). https://doi.org/10.1016/S0038-1098(98)00162-8
49. A. Gadisa, K. Tvingstedt, K. Vandewal, F. Zhang, J.V. Manca, O. Inganäs, Bipolar charge transport in fullerene molecules in a

bilayer and blend of polyfluorene copolymer and fullerene. Adv. Mater. **22**, 1008–1011 (2010). https://doi.org/10.1002/adma.200902579
50. D. Bartesaghi, M. Turbiez, L.J.A. Koster, Charge transport and recombination in PDPP5T:[70]PCBM organic solar cells: the influence of morphology. Org. Electron. **15**, 3191–3202 (2014). https://doi.org/10.1016/j.orgel.2014.08.064
51. D. Yang, X. Zhang, K. Wang, C. Wu, R. Yang, Y. Hou, Y. Jiang, S. Liu, S. Priya, Stable efficiency exceeding 20.6% for inverted perovskite solar cells through polymer-optimized PCBM electron-transport layers. Nano Lett. **19**, 3313–3320 (2019). https://doi.org/10.1021/acs.nanolett.9b00936
52. A. Turut, A. Karabulut, K. Ejderha, N. Bıyıklı, Capacitance–conductance–current–voltage characteristics of atomic layer deposited Au/Ti/Al2O3/n-GaAs MIS structures. Mater. Sci. Semicond. Process. **39**, 400–407 (2015). https://doi.org/10.1016/j.mssp.2015.05.025
53. B.A. Prew, Physics of semiconductor devices. Phys. Bull. **26**, 399–403 (1975). https://doi.org/10.1088/0031-9112/26/9/031
54. S. Demirezen, Ş Altlndal, Y. Azizian-Kalandaragh, A.M. Akbaş, A comparison of Au/n-Si Schottky diodes (SDs) with/without a nanographite (NG) interfacial layer by considering interlayer, surface states (Nss) and series resistance (Rs) effects. Phys. Scr. **97**, 055811 (2022). https://doi.org/10.1088/1402-4896/ac645f
55. H.G. Çetinkaya, S. Demirezen, S. Altındal Yerişkin, Electrical parameters of Au/(%1Ni-PVA)/n-Si (MPS) structure: surface states and their lifetimes. Phys. B Condens. Matter **621**, 413207 (2021). https://doi.org/10.1016/j.physb.2021.413207
56. S. Altındal Yerişkin, Y. Şafak Asar, Influence of graphene doping rate in PVA organic thin film on the performance of Al/p-Si structure. J. Mater. Sci. Mater. Electron. **32**, 22860–22867 (2021). https://doi.org/10.1007/s10854-021-06763-z
57. M. Yıldırım, M.O. Erdal, A. Kocyigit, The effect of indium doping concentration on the electrical and dielectric properties of Al/In:ZnO/p-Si heterojunctions. Phys. B Condens. Matter **572**, 153–160 (2019). https://doi.org/10.1016/j.physb.2019.07.055
58. A.A.M. Farag, B. Gunduz, F. Yakuphanoglu, W.A. Farooq, Controlling of electrical characteristics of Al/p-Si Schottky diode by tris(8-hydroxyquinolinato) aluminum organic film. Synth. Met. **160**, 2559–2563 (2010). https://doi.org/10.1016/j.synthmet.2010.10.005
59. M. Yildirim, A. Kocyigit, A systematic study on the dielectric relaxation, electric modulus and electrical conductivity of Al/Cu:TiO2n -Si (MOS) structures/capacitors. Surf. Rev. Lett. **27**, 1950217 (2020). https://doi.org/10.1142/S0218625X19502172
60. W.A. Hill, C.C. Coleman, A single-frequency approximation for interface-state density determination. Solid. State. Electron. **23**, 987–993 (1980). https://doi.org/10.1016/0038-1101(80)90064-7
61. E.H. Nicollian, J.R. Brews, *MOS (metal oxide semiconductor) physics and technology* (John Wiley & Sons, Somerset, 2003)
62. Ç. Bilkan, Ş Altındal, Y. Azizian-Kalandaragh, Investigation of frequency and voltage dependence surface states and series resistance profiles using admittance measurements in Al/p-Si with Co3O4-PVA interlayer structures. Phys. B Condens. Matter **515**, 28–33 (2017). https://doi.org/10.1016/J.PHYSB.2017.04.002
63. S. Zeyrek, E. Acaroğlu, Ş Altındal, S. Birdoğan, M.M. Bülbül, The effect of series resistance and interface states on the frequency dependent C-V and G/w–V characteristics of Al/perylene/p-Si MPS type Schottky barrier diodes. Curr. Appl. Phys. **13**, 1225–1230 (2013). https://doi.org/10.1016/j.cap.2013.03.014
64. M. Yıldırım, Characterization of the framework of Cu doped TiO2 layers: An insight into optical, electrical and photodiode parameters. J. Alloys Compd. **773**, 890–904 (2019). https://doi.org/10.1016/J.JALLCOM.2018.09.276
65. A. Kocyigit, M. Yıldırım, A. Sarılmaz, F. Ozel, The Au/Cu2WSe4/p-Si photodiode: electrical and morphological characterization. J. Alloys Compd. **780**, 186–192 (2019). https://doi.org/10.1016/j.jallcom.2018.11.372
66. M.O. Erdal, A. Kocyigit, M. Yıldırım, The rate of Cu doped TiO2 interlayer effects on the electrical characteristics of Al/Cu:TiO2/n-Si (MOS) capacitors depend on frequency and voltage. Microelectron. Reliab. **106**, 113591 (2020). https://doi.org/10.1016/j.microrel.2020.113591
67. U.K. Verma, S. Kumar, Y.N. Mohapatra, Measurement of contact surface photo-voltage from forward bias C-V characteristics of P3HT:PCBM based BHJ solar cells. Sol. Energy Mater. Sol. Cells **172**, 25–33 (2017). https://doi.org/10.1016/j.solmat.2017.07.010